



# ERNEST ORLANDO LAWRENCE BERKELEY NATIONAL LABORATORY

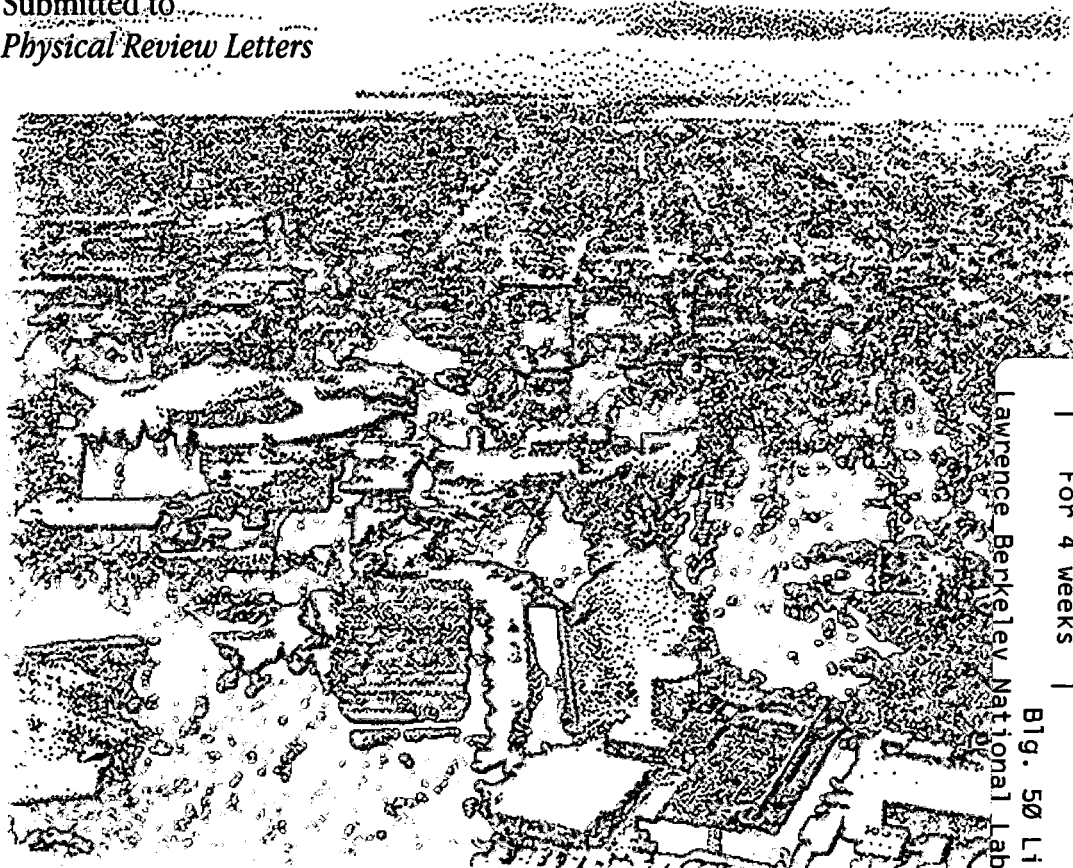
## Observation of the Angular Distribution of Photofragment Alignment

Allan S. Bracker, Eloy R. Wouters,  
Arthur G. Suits, Yuan T. Lee, and  
Oleg S. Vasyutinskii

**Chemical Sciences Division**

July 1997

Submitted to  
*Physical Review Letters*



Lawrence Berkeley National Laboratory

LOAN COPY  
Circulates  
For 4 weeks

Copy 2

Big. 50 Lib Rm 4014

LBNL-40480

## **DISCLAIMER**

This document was prepared as an account of work sponsored by the United States Government. While this document is believed to contain correct information, neither the United States Government nor any agency thereof, nor the Regents of the University of California, nor any of their employees, makes any warranty, express or implied, or assumes any legal responsibility for the accuracy, completeness, or usefulness of any information, apparatus, product, or process disclosed, or represents that its use would not infringe privately owned rights. Reference herein to any specific commercial product, process, or service by its trade name, trademark, manufacturer, or otherwise, does not necessarily constitute or imply its endorsement, recommendation, or favoring by the United States Government or any agency thereof, or the Regents of the University of California. The views and opinions of authors expressed herein do not necessarily state or reflect those of the United States Government or any agency thereof or the Regents of the University of California.

## **Observation of the Angular Distribution of Photofragment Alignment**

Allan S. Bracker,<sup>a,b</sup> Eloy R. Wouters,<sup>b</sup> Arthur G. Suits,<sup>b</sup>  
Yuan T. Lee,<sup>a,b,c</sup> and Oleg S. Vasyutinski<sup>d</sup>

<sup>a</sup>Department of Chemistry, University of California, Berkeley, CA 94720

<sup>b</sup>Chemical Sciences Division, Ernest Orlando Lawrence Berkeley National Laboratory,  
University of California, Berkeley, California 94720

<sup>c</sup>Academia Sinica, Nankang, Taipei 11529, Taiwan

<sup>d</sup>Ioffe Physico-Technical Institute, Russian Academy of Sciences,  
194021 St. Petersburg, Russia

July 1997

# Observation of the angular distribution of photofragment alignment

Allan S. Bracker<sup>a,b</sup>, Eloy R. Wouters<sup>b</sup>, Arthur G. Suits<sup>b,\*</sup>, Yuan T. Lee<sup>a,b,c</sup> and  
Oleg S. Vasyutinskii<sup>d,\*</sup>

<sup>a</sup> *Department of Chemistry, University of California, Berkeley, CA 94720*

<sup>b</sup> *Chemical Sciences Division, Ernest Orlando Lawrence Berkeley National Laboratory, Berkeley,  
CA 94720*

<sup>c</sup> *Academia Sinica, Nankang, Taipei 11529, Taiwan*

<sup>d</sup> *Ioffe Physico-Technical Institute, Russian Academy of Sciences, 194021 St. Petersburg, Russia*

## Abstract

The recoil-angle dependence of ground state chlorine atom angular momentum alignment was measured for the dissociation of chlorine molecules with 355 nm light. This dependence is seen explicitly in ion image data, which map the three-dimensional velocity vector distribution of state-selectively ionized photofragments into a two-dimensional spatial distribution. The pure alignment signal is isolated from the much larger population signal by taking appropriate linear combinations of data sets with different dissociation and probe laser polarizations. Qualitative comparison of the data images with a theoretical simulation clearly shows both incoherent and coherent contributions to a perpendicular optical transition in the parent molecule. We outline a general approach to the extraction of dynamical information from ion image

---

\*Corresponding authors

data obtained with two-photon excitation as the photofragment probe.

PACS numbers: 33.80.Gj, 34.50.Gb, 34.50.Lf

Photofragment angular momentum polarization is a detailed signature of molecular photodissociation dynamics. For the case of atomic photofragments, this polarization provides information on the electronic rearrangement which occurs during optical excitation and dissociation of the parent molecule. Several factors contribute to this polarization [1–4]. For the idealized case of a diatomic system which dissociates on a single adiabatic potential energy curve, only the electronic state symmetry and the associated Coulomb interaction at large interatomic distance will govern the polarization. However in general, multiple molecular electronic states are involved, both in the initial excitation and during the course of dissociation. They are individually expected to yield different atomic polarizations, and coherent excitation of two or more states can lead to strong interference effects. Finally, nonadiabatic transitions between electronic states will mix the contributions of individual states.

The most detailed dynamical information is obtained by measuring the fragment angular momentum polarization as a function of recoil angle ( $\mathbf{v}$ - $\mathbf{j}$  correlation). In recent years, a number of such studies have been carried out for the case of diatomic photofragments with rotational angular momentum. For the high angular momenta which are routine in these polyatomic systems, there exists a very convenient semiclassical formalism to describe the  $\mathbf{v}$ - $\mathbf{j}$  correlation by making use of a bipolar harmonic expansion [5]. Although this widely-used method can be adapted for low rotational states, there now exists a fully quantum mechanical treatment which makes use of parameters with explicit dynamical significance [6]. This approach is especially useful for the low values of the electronic angular momentum quantum numbers encountered in investigations of polarized atomic photofragments. To date, there are relatively few reports of  $\mathbf{v}$ - $\mathbf{j}$  correlation measurements for atomic photofragments [7,8], and none yet have provided a rigorous means for extracting and describing the polarization angular distribution.

Experimentally, one must measure both the recoil velocity vector and the correlated angular momentum polarization. Sensitivity to angular momentum polarization is easily obtained via laser-based spectroscopic probes such as Laser-Induced Fluorescence (LIF) or

Resonance-Enhanced Multiphoton Ionization (REMPI). The velocity vector distribution can be resolved by measuring Doppler profiles or Time-of-Flight mass spectrometric peak profiles (one-dimensional projections) or photofragment ion images (two-dimensional projection). Two-dimensional ion imaging has the advantage of reducing the number of experimental geometries that must be used to reconstruct the three-dimensional distribution.

We obtained the data presented in this report with a standard ion imaging apparatus, shown schematically in Fig. 1. In each cycle of the experiment, a pulsed supersonic expansion of chlorine gas (10% seeded in Argon) was crossed at  $90^\circ$  by counter-propagating linearly-polarized laser beams. The first laser pulse (355 nm) dissociated a small fraction of the  $\text{Cl}_2$  molecules contained in the intersection volume of the laser and the molecular beam. The second laser pulse (234.336 nm) state-selectively ionized the nascent chlorine atoms using 2+1 REMPI [ $\text{Cl}^+ \leftarrow \text{Cl}(4p^2D_{3/2}^\circ) \leftarrow \leftarrow \text{Cl}(3p^2P_{3/2}^\circ)$ ]. Under the laser power density conditions necessary to drive the two-photon transition, the ionization step was easily saturated and thus insensitive to angular momentum polarization.

The ions produced in each laser shot were extracted by an electric field into a field-free flight tube. During the  $9 \mu\text{s}$  flight time, the chlorine ion packet expands to a diameter of 3 cm due to the recoil energy released in the dissociation. At the end of the flight tube, the expanded packet strikes the surface of a microchannel plate which is gated to detect only the  $\text{Cl}^+$  mass. Electrons emerging from the back of the microchannel plate impinge on a phosphor screen to produce images which are collected and signal-averaged with a video camera. To further improve the signal-to-noise ratio, we used an image processor to combine the raw data images with their horizontal and vertical reflections.

In order to obtain complete information about the velocity and alignment anisotropy, we used four different combinations of the dissociation and probe light polarization vectors. The dissociation laser polarization was either parallel or perpendicular to the ion flight axis (Z-axis), which we refer to as Geometries I and II, respectively. The probe laser polarization was either parallel or perpendicular to the dissociation laser polarization. The four corresponding images are presented in Fig. 2.

Ion images are projections onto the detector plane of a three-dimensional distribution of ions. The dominant contribution to the shape of this distribution is the well-known photofragment velocity anisotropy, described by the expression  $P(\theta) \propto 1 + \beta P_2(\cos \theta)$ , where  $\theta$  is the polar recoil angle with respect to the dissociation laser polarization. At 355 nm, the perpendicular optical transition  ${}^1\Pi_{1_u} \leftarrow {}^1\Sigma_{0_g^+}$  contributes more than 90% of the light absorption [9], so the anisotropy parameter  $\beta$  is close to its limiting value of  $-1$ . The coarse image shapes for Geometries I and II represent two different projections of  $P(\theta)$ .

The smaller modulations in the images are of greater significance for this report. The sign of these modulations depends on the probe laser polarization, thus they are most easily seen by contrasting the images in Fig. 1 (top vs. bottom), or by viewing the weighted differences shown in Fig. 4 (top). This variation of the two-photon detection sensitivity with laser polarization is a direct result of angular momentum alignment.

Another manifestation of photofragment angular momentum alignment is that the total signal intensity depends on the relative polarizations of the dissociation and probe lasers. It can be shown that the total photofragment alignment parameter  $A_{20}$  is proportional to the difference between these intensities [10]. In our experiment, this difference was  $A_{20} \propto (\langle I_Z \rangle - \langle I_Y \rangle) / (\langle I_Z \rangle + 2\langle I_Y \rangle) = -0.035 \pm 0.01$ , where  $Z$  and  $Y$  refer to the linear polarization axis of the probe laser, and the angle brackets indicate averaging over all recoil directions.

Angular momentum polarization can be conveniently described in terms of irreducible density matrix components (state multipoles) [10,11]. For the case of molecular dissociation, the photofragment state multipoles are a function of recoil angles, i.e.  $\rho_{kq} = \rho_{kq}(\theta, \phi)$ . The  $\rho_{00}(\theta, \phi)$  term represents the angular distribution of photofragment density, while terms with rank  $k > 0$  allow for the  $\mathbf{v}$ - $\mathbf{j}$  correlation. As shown in a recent theoretical analysis [6], all combinations of the indices  $k$  and  $q$  (i.e.  $k=0 \dots 2j$ ,  $q=-k \dots k$ ) should generally be assumed to be non-zero. Even for linearly polarized dissociation light, it is possible to produce angle-dependent multipoles with odd  $k$  (orientation). However, a linearly polarized two-photon optical probe is capable of detecting only alignment moments with  $k=0, 2$  and  $4$ . Given these considerations, for this report only rank  $k=0$  (photofragment density) and  $k=2$  (quadrupolar

alignment) multipoles are of importance.

Since the absorption intensity modulation due to alignment is typically much smaller than the total absorption intensity, it is useful to isolate the alignment contribution by choosing linear combinations of images for which the  $\rho_{00}(\theta, \phi)$  term disappears. Also, by combining three orthogonal probe polarization geometries, the alignment-independent part of the signal can be obtained. For a two-photon probe, the general expressions for these combinations are

$$I_{X,Y} - I_Z = \frac{C}{\sqrt{2}} R_2 \left\{ \rho_{20}(\theta, \phi) \mp \sqrt{\frac{2}{3}} \text{Re} [\rho_{22}(\theta, \phi)] \right\} \quad (1a)$$

$$I_Y - I_X = \frac{2C}{\sqrt{3}} R_2 \text{Re} [\rho_{22}(\theta, \phi)] \quad (1b)$$

$$I_X + I_Y + I_Z = C R_0 \rho_{00}(\theta, \phi), \quad (1c)$$

where the signs  $-$  and  $+$  in Eq. (1a) refer to  $I_X$  and  $I_Y$ , respectively, and  $C$  is a constant. Note that for the experimental geometries chosen here,  $\rho_{21}$  and  $\text{Im}(\rho_{22})$  do not contribute to the signal. The coefficients  $R_k$  in Eq. (1) are similar to the linestrength moments  $P_q^k$  of Ref. [12], except that the laser polarization dependence has been factored out and evaluated. In principle, all three measurable alignment multipoles may be isolated by an appropriate combination of images, although in practice it may be difficult to obtain images for certain geometries, due to limitations in the experimental apparatus.

In order to project the three-dimensional intensity distribution onto two dimensions, we used the transformation

$$M(\rho, \phi) = 2 \int_{\rho}^{\infty} \frac{f(\arcsin(\rho/r), \phi) g(r)}{\sqrt{1 - \rho^2/r^2}} dr, \quad (2)$$

where  $M(\rho, \phi)$  is the image,  $(\rho, \phi)$  are polar coordinates, and  $r$  is the modulus of the photofragment radius-vector. The function  $f(\arcsin(\rho/r), \phi) \equiv f(\theta, \phi)$  in Eq. (2) describes the angular dependence of the intensity distribution and can be substituted with one of the intensity differences in Eq. (1). The function  $g(r)$  describes the radial dependence of the three-dimensional distribution, which is a delta function for this work, since the chlorine atom photofragments are monoenergetic. Eq. (2) assumes reflection symmetry of the

function  $f(\arcsin(\rho/r), \phi)$  in the X–Y plane. Unlike the Abel transform, Eq. (2) cannot be directly inverted to reconstruct the three-dimensional ion distribution from image data. Although, the inverse-Abel transform is widely used for this purpose [13], it requires as input the projections of cylindrically symmetric distributions with the symmetry axis parallel to the detector plane. These geometric restrictions are often violated in experiments designed to measure a  $\mathbf{v}\text{-j}$  correlation.

The integral in Eq. (2) can be evaluated analytically for the case of  $g(r) = \delta(r - r_0)$ , where  $r_0 = v_0\tau$ ,  $v_0$  is the photofragment velocity, and  $\tau$  is the flight time of the ions. We show explicit results only for the  $I_Z\text{-}I_Y$  case used in our experiments. For dissociation polarization geometries I and II, using Eq. (1a) for  $f$  in Eq. (2) yields

$$M_{YZ}^I(t, \phi) \propto \frac{2}{\sqrt{1-t^2}} \{ [s_2 - 2\alpha_2 + 3\alpha_2 t^2][1 - t^2(1 + \sin^2 \phi)] - 2\gamma_2 t^2(1 - t^2)(1 + \sin^2 \phi) - \frac{\eta_2}{4} t^2 [t^2 + (2 - t^2) \cos(2\phi)] \}, \quad (3a)$$

and

$$M_{YZ}^{II}(t, \phi) \propto \frac{2}{\sqrt{1-t^2}} \{ [s_2 + \alpha_2(1 - 3t^2 \sin^2 \phi)][1 - t^2(1 + \sin^2 \phi)] + 2\gamma_2 t^2 \sin^2 \phi [2 - t^2(1 + \sin^2 \phi)] + \frac{\eta_2}{2} [t^2(2 - t^2) \cos(2\phi) + 1 - t^2 + t^4(1 - \frac{\sin^2(2\phi)}{4})] \}. \quad (3b)$$

The variable  $t$  is the radial coordinate normalized to the maximum possible radius, i.e.  $t = \rho/r_0$ .

The anisotropy parameters  $s_2$ ,  $\alpha_2$ ,  $\gamma_2$  and  $\eta_2$  in Eq. (3), which characterize the alignment angular distribution, are a subset of the polarization anisotropy parameters defined in Ref. [14]. They are normalized combinations of the theoretically-derived ‘dynamical functions’  $f_k(q, q')$  [4,6]. (General expressions for the angle-dependent state multipoles in terms of  $f_k(q, q')$  can be found in Ref. [6].) These new anisotropy parameters have a clear physical interpretation as contributions to the total photofragment orientation and alignment parameters  $A_{T0}$  and  $A_{20}$  from incoherent and coherent excitation mechanisms.

Eqs (3) provide a powerful means for interpreting the alignment contribution to photofragment ion image data, since each of four alignment mechanisms is associated with

a unique radial and angular dependence in the images. This important fact is emphasized in Fig. 3, where each spatial dependence is shown in isolation. The calculated images of Fig. 3(a) show the contribution of a pure perpendicular optical transition ( $|\Omega - \Omega_0| = 1$ , where  $\Omega_0$  and  $\Omega$  are projections of the total angular momentum onto the internuclear axis for ground and excited states, respectively). Fig. 3(a) was obtained by setting  $s_2 = 2\alpha_2$  and the other parameters to zero. Fig. 3(b) corresponds to a pure parallel transition ( $\Omega - \Omega_0 = 0$ ) and was obtained by setting  $s_2 = -\alpha_2$  and the other parameters to zero. The above relationships between  $s_2$  and  $\alpha_2$  are apparent from their definitions in terms of dynamical functions [14]. Parameter  $\eta_2$  corresponds to coherent perpendicular excitation ( $\Omega = \pm 1$ ) [Fig. 3(c)], while  $\gamma_2$  corresponds to coherent excitation via both parallel and perpendicular transitions [Fig. 3(d)].

The data images in Fig. 2 were subtracted as prescribed by Eq. (1a). These differences and qualitative fits are shown in Fig. 4. Both perpendicular incoherent and coherent contributions were required to obtain satisfactory fits. The ratio of alignment anisotropy parameters  $\alpha_2/\eta_2$  was  $-1.5$ . The presence of the incoherent perpendicular contribution is completely consistent with previous investigations of chlorine dissociation [9], however, direct evidence for a coherent contribution is presented here for the first time. In order to determine the sign and absolute values of the alignment anisotropy parameters, as well as the absolute degree of  $\text{Cl}(^2\text{P}_{3/2}^\circ)$  alignment, it will be necessary to calculate the linestrength coefficients  $R_k$ .

In summary, we have shown that for the case of chlorine photodissociation, the atomic alignment angular distribution explicitly reveals the electronic state symmetries and coherence effects. The latter cannot be directly obtained from measurements of velocity anisotropy or spin-orbit branching ratios. We have derived general expressions for the alignment contribution to photofragment ion images. These expressions provide a direct connection between experimental observables and important theoretical quantities. Measurements of orientation and alignment at higher image spatial resolution should permit an even more detailed assignment of the electronic states and nonadiabatic transitions involved in photodissociation.

This work was supported by the Director, Office of Energy Research, Office of Basic

Energy Sciences, Chemical Sciences Division of the U.S. Department of Energy under Contract No. DE-AC03-76SF00098, and by a Cooperative Grant from the Civilian Research and Development Fund, CRDF Award No. RP1-223.

## REFERENCES

- [1] S.J. Singer, K.F. Freed, and Y.B. Band, *J. Chem. Phys.* **79**, 6060 (1983).
- [2] J. Vigué, J.A. Beswick, and M. Broyer, *J. Physique* **44**, 1225 (1983).
- [3] M. Glass-Maujean and J.A. Beswick, *J. Chem. Soc. Faraday Trans.* **85**, 983 (1989).
- [4] D.V. Kupriyanov and O.S. Vasyutinskii, *Chem. Phys.* **171**, 25 (1993).
- [5] R.N. Dixon, *J. Chem. Phys.* **85**, 1866 (1986).
- [6] L.D.A. Siebbeles, M. Glass-Maujean, O.S. Vasyutinskii, J.A. Beswick, and O. Roncero, *J. Chem. Phys.* **100**, 3610 (1994).
- [7] Y. Wang, H.P. Looock, J. Cao, and C.X.W. Qian, *J. Chem. Phys.* **102**, 808 (1995).
- [8] Y. Mo, H. Katayanagi, M.C. Heaven, and T. Suzuki, *Phys. Rev. Lett.* **77**, 830 (1996).
- [9] Y. Matsumi, K. Tonokura, and M. Kawasaki, *J. Chem. Phys.* **97**, 1065 (1992).
- [10] R.N. Zare, *Angular Momentum* (World Scientific, New York, 1988).
- [11] K. Blum, *Density Matrix Theory and Applications* (Plenum Press, New York, 1989).
- [12] A.C. Kummel, G.O. Sitz, and R.N. Zare, *J. Chem. Phys.* **85**, 6874 (1986); **88**, 6707 (1987).
- [13] R.N. Strickland and D.W. Chandler, *Appl. Opt.* **30**, 1811 (1991).
- [14] B.V. Picheyev, A.G. Smolin, and O.S. Vasyutinskii, *J. Phys. Chem.* (to be published).

## FIGURES

FIG. 1. Schematic of experimental apparatus. The cartesian axis definition in this figure is used throughout the paper.

FIG. 2. Chlorine photofragment ion images. Geometries I and II correspond to the dissociation laser polarization along the Z and Y axes, respectively. Geometries I and II were each probed with the probe laser polarization along the Z and Y axes.

FIG. 3. (color) Plots of  $M_{YZ}(t, \phi)$  [Eq. (3)] for dissociation polarization geometries I and II. Cases (a)–(d) correspond to four mechanistic limits as follows: (a) incoherent perpendicular excitation, (b) incoherent parallel excitation, (c) coherent perpendicular excitation, (d) coherent parallel and perpendicular excitation. Blue and red correspond to positive and negative values, respectively.

FIG. 4. (color) Contribution of photofragment alignment to data signal (top row) and qualitative simulation (bottom row) based on Eq. (3). Only contributions from perpendicular transitions [Fig. 3(a) and 3(c)] were included. See text for details.

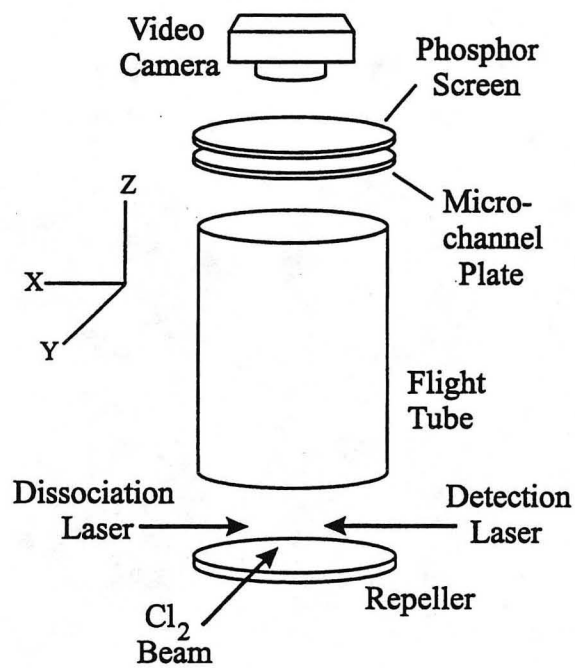


Figure 1

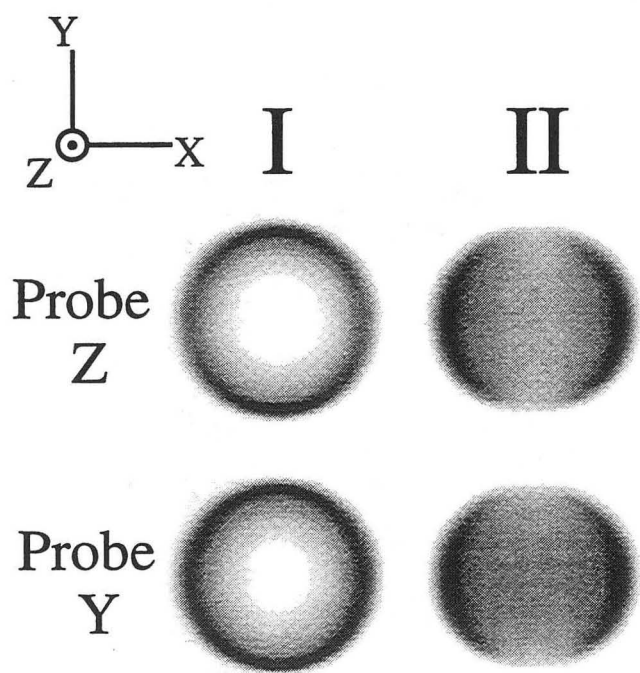


Figure 2

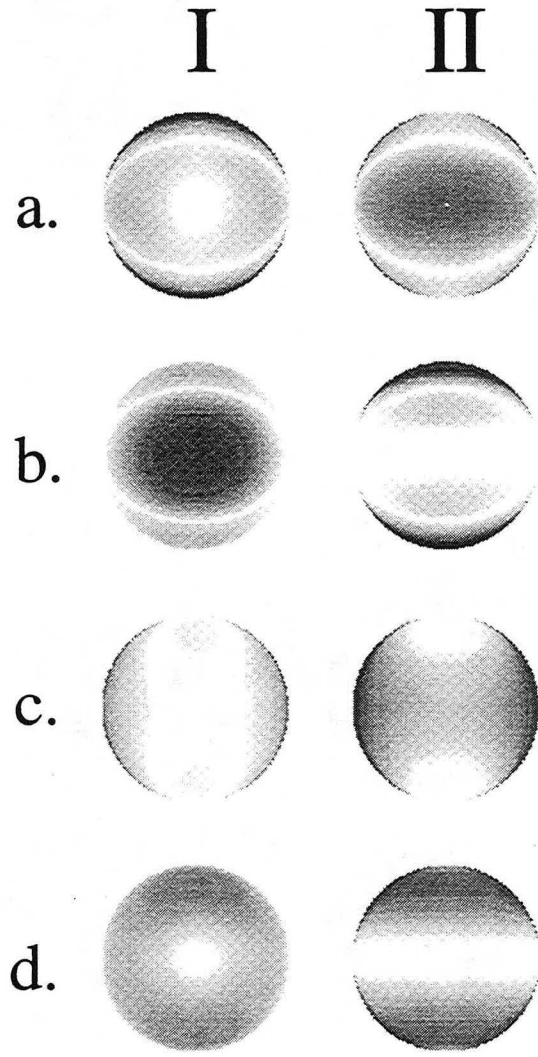


Figure 3

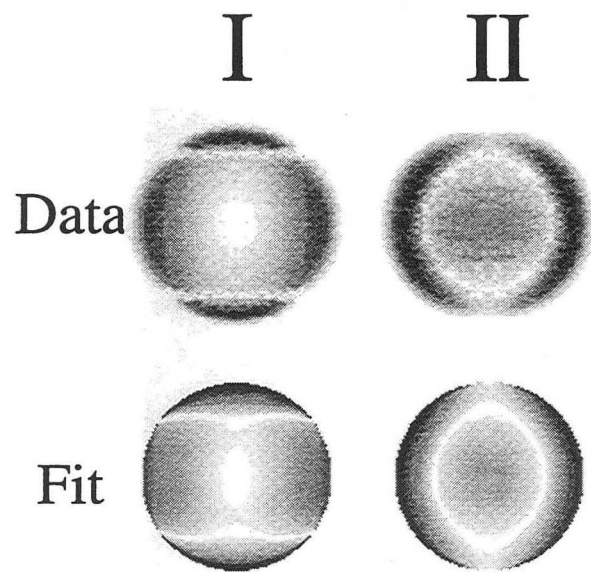


Figure 4

**ERNEST ORLANDO LAWRENCE BERKELEY NATIONAL LABORATORY  
ONE CYCLOTRON ROAD | BERKELEY, CALIFORNIA 94720**

**AAY313**



**LBL Libraries**